Asymptotic High-Frequency Green's Function for a Large Rectangular Planar Periodic Phased Array of Dipoles With Weakly Tapered Excitation in Two Dimensions

F. Mariottini, F. Capolino, *Senior Member, IEEE*, S. Maci, *Fellow, IEEE*, and L. B. Felsen, *Life Fellow, IEEE*

***Abstract*—This paper deals with the derivation and physical interpretation of a uniform high-frequency representation of the Green's function for a large planar rectangular phased array of dipoles with weakly varying excitation. Thereby, our earlier published results, valid for equiamplitude excitation, and those for tapered illumination in one dimension are extended to tapering along *both* dimensions, including dipole amplitudes tending to zero at the edges. As previously, the field obtained by direct summation over the contributions from the individual radiators is restructured into a double spectral integral whose high-frequency asymptotic reduction yields a series of propagating and evanescent Floquet waves (FWs) together with corresponding FW-modulated diffracted fields, which arise from FW scattering at the array edges and vertexes. To accommodate the weak amplitude tapering, new generalized periodicity-modulated edge and vertex "slope" transition functions are introduced, accompanied by a systematic procedure for their numerical evaluation. Special attention is given to the analysis and physical interpretation of the complex vertex diffracted ray fields. A sample calculation is included to demonstrate the accuracy of the asymptotic algorithm. The resulting array Green's function forms the basic building block for the full-wave analysis of planar weakly amplitude-tapered phased array antennas, and for the description of electromagnetic radiation and scattering from weakly amplitude-tapered rectangular periodic structures.**

***Index Terms*—Floquet expansions, Green's functions, periodic structures, phased array antennas.**

I. Introduction

In A systematic sequence of previous studies [1]–[5], we have explored methods to reduce the often prohibitive numerical effort that accompanies an element-by-element full-wave analysis of large truncated plane periodic phased arrays. In our approach, the element-by-element array Green's function (AGF) formed by a planar periodic phased array of dipoles is restructured into an alternative "collective" formulation that represents the field radiated from the elementary dipoles in terms of the radiation from a superposition of continuous truncated Floquet wave (FW)-matched source distributions extending over the entire aperture of the array, with inclusion of other truncation-induced Floquet-modulated wave types. Since the FW series exhibits excellent convergence properties when the observation point is located far enough away from the array surface to render evanescent FWs and the corresponding diffracted fields negligible, this representation has been found to be more efficient than the direct summation of the spatial contributions from each element of the array, especially when each FW aperture distribution is treated asymptotically. The previous investigations have dealt with semi-infinite planar dipole arrays [1], [2] and right-angle sectoral planar phased arrays of dipoles [3], [4] with equiamplitude excitation, as well as strip arrays with one direction-tapered illumination [5].

Our new extension in this paper addresses planar rectangular arrays with slowly varying excitation profiles that are separable in the two orthogonal variables. The corresponding asymptotic treatment of each FW aperture distribution leads to locally amplitude-modulated truncated FWs, plus FW-excited diffracted contributions from the edges and vertexes of the array, which can be cast as previously in the format of a periodicity-adapted geometrical theory of diffraction (GTD). For the canonical finite planar phased array of dipoles with tapered excitation, the AGF is constructed by plane wave spectral decomposition in the two-dimensional complex wavenumber domain corresponding to the array-plane coordinates. This is followed by manipulations and contour deformations that prepare the integrands for subsequent efficient and physically incisive asymptotics parameterized by critical spectral points, i.e., saddle points and points at which the spectral amplitude function exhibits highly peaked characteristics very similar to those of poles (denoted later on as "quasi-poles"). Different species of spectral quasi-poles define the various species of propagating and evanescent locally amplitude-modulated FWs. The other critical points in the double spectral integral define the asymptotic behavior of the edge and vertex diffracted rays; the confluence of these critical points in transition regions determines a variety of locally uniform new transition functions for truncated edge diffracted and vertex diffracted waves.

Arrays with tapered excitation have also been analyzed in [6], combining "global" FWs and diffracted fields developed in [1]–[3] with a numerical technique based on the discrete Fourier

Manuscript received October 6, 2003; revised July 19, 2004. The work of F. Mariottini, F. Capolino, and S. Maci was supported by the European Space Agency, The Netherlands. The work of L. B. Felsen was supported in part by Polytechnic University, Brooklyn, NY.

F. Mariottini, F. Capolino, and S. Maci are with the Department of Information Engineering, University of Siena, Siena 53100, Italy (e-mail: macis@ing.unisi.it).

L. B. Felsen is with the Department of Aerospace and Mechanical Engineering and Department of Electrical and Computer Engineering, Boston University, Boston, MA 02215 USA (e-mail: lfelsen@bu.edu).

Digital Object Identifier 10.1109/TAP.2004.841321

transform (DFT) that expands a general tapering in terms of its equiamplitude phased harmonics. Although the numerical DFT procedure can be applied to a wider class of taperings, our results here are in analytical closed form and thus can be rapidly computed for the considered class of applications [7]–[9].

II. Statement of the Problem

Consider a large rectangular periodic array of $N_1 \times N_2$ linearly phased dipoles located in the z_1, z_2 plane (Fig. 1). The array dimensions are L_1 and L_2 along z_1 and z_2, respectively; the interelement spatial periods along the z_1 and z_2 directions are given by d_1 and d_2; and the interelement phase gradients of the excitation by γ_1 and γ_2, respectively. An $\exp(j\omega t)$ dependence is implied and suppressed. All dipoles are oriented along the unit vector $\hat{\mathbf{J}}_0$ (boldface symbols denote vector quantities, and boldface symbols with a caret ˆ denote unit vectors). Superimposed upon that background is a z-dependent amplitude-separable tapering function $f(z_1, z_2) = f_1(z_1) f_2(z_2)$, sampled at the dipole locations

$$\mathbf{J}(n_1 d_1, n_2 d_2) = \hat{\mathbf{J}}_0 f_1(n_1 d_1) f_2(n_2 d_2) e^{-j(\gamma_1 n_1 d_1 + \gamma_2 n_2 d_2)} \tag{1}$$

with $\mathbf{J}(z_1', z_2')$ denoting the dipole current amplitude, and $(z_1', z_2') = (n_1 d_1, n_2 d_2)$ denoting the location of (n_1, n_2)-th dipole. Without compromising practical utility, we assume $f(z_1, z_2)$ real and positive in the domain $z_1 \in [0, L_1], z_2 \in [0, L_2]$, and zero elsewhere; here, $L_1 = (N_1 - 1)d_1$ and $L_2 = (N_2 - 1)d_2$. The electromagnetic vector field at any observation point $\mathbf{r} = z_1 \hat{\mathbf{z}}_1 + z_2 \hat{\mathbf{z}}_2 + y\hat{\mathbf{y}}$ can be derived from the magnetic vector potential

$$\mathbf{A}(\mathbf{r}) = \sum_{n_1=0}^{N_1-1} \sum_{n_2=0}^{N_2-1} \frac{e^{-jkR_{n_1,n_2}}}{4\pi R_{n_1,n_2}} \mathbf{J}(n_1 d_1, n_2 d_2) \tag{2}$$

where $R_{n_1,n_2} = \sqrt{(z_1 - n_1 d_1)^2 + (z_2 - n_2 d_2)^2 + y^2}$, which is synthesized by summing over the individual (n_1, n_2) dipole radiations. Our goal is the efficient and phenomenologically insightful evaluation of the high-frequency near and far fields radiated by this complex physical configuration.

III. Formal Solution and High-Frequency Parameterizations

A. Spectral Domain Analysis: Floquet Waves

Our analysis is carried out in the spectral wavenumber domain. Accordingly, we employ the spectral Fourier representation of the scalar free space Green's function $e^{-jkR(z_1,z_2)}/[4\pi R(z_1, z_2)]$ with $R(z_1, z_2) = \sqrt{z_1^2 + z_2^2 + y^2}$; this Fourier transform is given by $e^{\mp jk_y y}/[2jk_y]$ [10], where $k_y = \sqrt{k^2 - k_{z_1}^2 - k_{z_2}^2}$ and the upper and lower signs apply to $y > 0$ and $y < 0$, respectively. Because of symmetry, from here on, we shall deal with $y > 0$ only. On the top Riemann sheet of the complex k_{z_1}-plane, for real k_{z_2}, we define $\Im m(k_y) < 0$ for $k^2 - k_{z_2}^2 < k_{z_1}^2$ and $k_y > 0$ for $k^2 - k_{z_2}^2 > k_{z_1}^2$. The location of branch points and branch cuts with respect to the real-axis integration path in the k_{z_1} plane is found by introducing small losses ($\Im m(k) = 0^-$), which are eventually removed [1], [3],

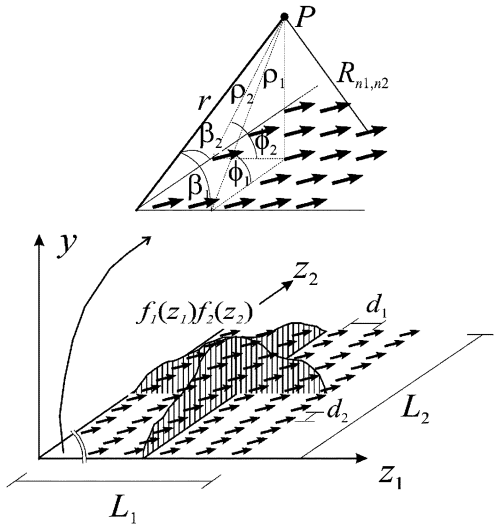

Fig. 1. $\hat{\mathbf{J}}_0$-directed parallel dipoles, weighted by an amplitude taper and linear phasing, with d_1 and d_2 denoting the interelement spatial periods along z_1 and z_2, respectively. The tapering function $f_1(z_1) f_2(z_2)$ is slowly varying with respect to the wavelength. The inset shows the local coordinate system associated with a vertex. Note that ρ_i is related to r by $r = \sqrt{\rho_i^2 + z_i^2}$ for $i = 1, 2$, respectively.

[4]. Substituting the spectral Fourier representation of the scalar free-space Green's function into (2) and interchanging the sequence of the (n_1, n_2)-summation and the spectral integration operations, leads to (see Section II for notation and definitions)

$$\mathbf{A}(\mathbf{r}) = \hat{\mathbf{J}}_0 A(\mathbf{r}) = \frac{\hat{\mathbf{J}}_0}{8\pi^2 j} \int_{-\infty}^{\infty} \int_{-\infty}^{\infty} \frac{e^{-jP(k_{z_1}, k_{z_2})}}{k_y} I_1(k_{z_1})\, I_2(k_{z_2})\, dk_{z_1} dk_{z_2} \tag{3}$$

where $P(k_{z_1}, k_{z_2}) = k_{z_1} z_1 + k_{z_2} z_2 + k_y y = \mathbf{k} \cdot \mathbf{r}$, with $\mathbf{k} = k_{z_1} \hat{\mathbf{z}}_1 + k_{z_2} \hat{\mathbf{z}}_2 + k_y \hat{\mathbf{y}}$ and

$$I_i(k_{z_i}) = \sum_{n_i=0}^{N_i-1} e^{j(k_{z_i} - \gamma_i) n_i d_i} f_i(n_i d_i), \quad i = 1, 2. \tag{4}$$

The (n_i)-sum I_1, I_2 in (4) is manipulated via the truncated Poisson sum formula [4], [11] into

$$I_i(k_{z_i}) = \frac{f_i(0)}{2} + \frac{f_i(L_i)}{2} e^{j(k_{z_i} - \gamma_i) L_i} + \frac{1}{d_i} \sum_{u=-\infty}^{\infty} \tilde{f}_i\left(k_{z_i} - k_{z_{i,u}}\right) \tag{5}$$

where

$$\tilde{f}_i\left(k_{z_i}'\right) = \int_0^{L_i} e^{jk_{z_i}' z_i} f_i(z_i) dz_i \tag{6}$$

are the Fourier-transformed tapering functions. The FW wavenumbers, which define the FW dispersion, are given by

$$k_{z_{1,q}} = \gamma_1 + \frac{2\pi q}{d_1}, \quad k_{z_{2,p}} = \gamma_2 + \frac{2\pi p}{d_2} \tag{7}$$

with $q, p = 0, \pm 1, \pm 2, \ldots$.

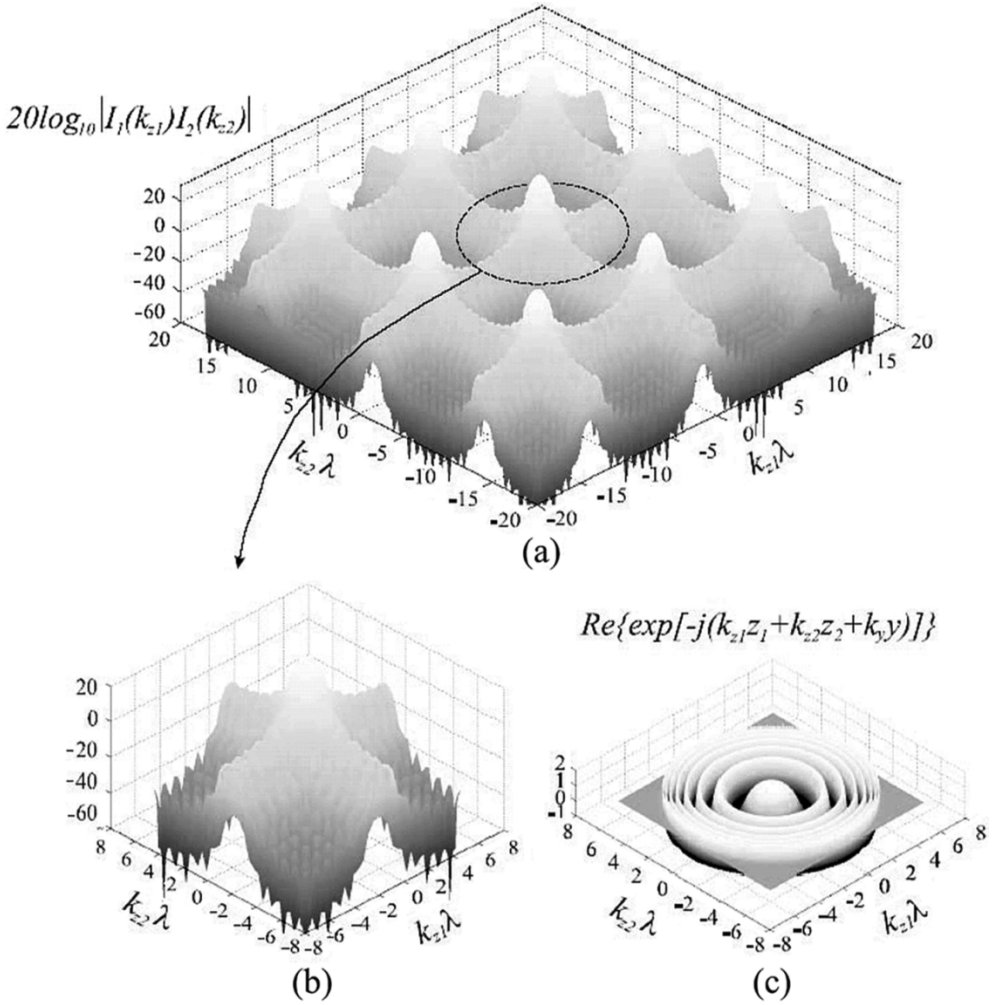

Fig. 2. Behavior of the SAF and the individual-element GF for a 30×30 element dipole array with $\gamma_i = 0, d_i = 0.5\lambda$, i.e., $k_{z_{i,u}} = (4\pi u/\lambda)$, with sine tapering $f_1(z_1) = \sin(\pi z_1/L_1), f_2(z_2) = \sin(\pi z_2/L_2)$. (a) Global SAF $= I_1(k_{z_1})I_2(k_{z_2})$; (b) typical SAF unit cell; (c) phase of individual-element GF. Since the tapering function has a wavenumber bandwidth narrow with respect to the spectral period, the aliasing of the spectra is small (outside the visible range, the oscillations are exponentially damped to zero).

B. Spectral Plane Inspection and Critical Points: High-Frequency Parameterizations

The integrand of (3) consists of two contributions that characterize the asymptotic behavior of the integral: the modulating spectral array factor (SAF) $I_1(k_{z_1})I_2(k_{z_2})$, and the spectral Green's function (GF) $(1/k_y)e^{-j\mathbf{k}\cdot\mathbf{r}}$. Henceforth, we assume (legitimately for realistic tapering functions on large arrays) that $f_i(z_i)$ varies slowly with respect to the wavelength λ (see Fig. 1). For this type of weak variation, and since $f_i(z_i)$ is positive in the domain $z_i \in [0, L_i]$, its spectrum $\tilde{f}_i(k'_{z_i})$ in (6) is localized around $k'_{z_i} = 0$. Since the function $I_i(k_{z_i})$ is synthesized by superposition of spectrum contributions translated to $k_{z_i} = k_{z_{i,u}}$ with $u = q$ or p for $i = 1$ or 2, respectively, this function appears concentrated around all the $k_{z_i} = k_{z_{i,u}}$ spectral points. For example, considering a 30×30 element dipole array with $\gamma_i = 0, d_i = 0.5\lambda$, i.e., $k_{z_{i,u}} = (2\pi u)/(d_i) = (4\pi u/\lambda)$, Fig. 2(a) and (b) displays the SAF $I_1(k_{z_1})I_2(k_{z_2})$ in (4) which appears in the integrand of (3), whereas Fig. 2(c) shows the rapid phase variation, with stationary phase at the center, of the *individual element* spectral Green's function $(1/k_y)e^{-j\mathbf{k}\cdot\mathbf{r}}$. On the basis of this decomposition, the behavior of the exact solution is parameterized by the critical points in the spectral double integral, which also govern the strategies for the asymptotic approximations. The critical points in (3) are the following.

i) $(k_{z_1}, k_{z_2}) = (k_{z_1,q}, k_{z_2,p})$. These points, where the SAF $I_1(k_{z_1})I_2(k_{z_2})$ in Fig. 2(a) exhibits peaks, describe the same phenomenology and localization property as the spectral poles for the semi-infinite array [2]. Accordingly, we shall refer to these points as *quasi-poles*.

ii) $(k_{z_1}, k_{z_2}) = (\bar{k}^s_{z_1}, \bar{k}^s_{z_2})$. This is a first-order two-dimensional stationary phase point (SPP) of the individual-element spectral GF in Fig. 2(c), which satisfies $(d/dk_{z_i})(\mathbf{k}\cdot\mathbf{r})_s = 0$ for $i = 1, 2$, with nonvanishing Hessian determinant, $|\det(d^2/dk_{z_i}dk_{z_j})(\mathbf{k}\cdot\mathbf{r})_s| \neq 0$. This SPP is related via $(\bar{k}^s_{z_1}, \bar{k}^s_{z_2}) = (k\cos\beta_1, k\cos\beta_2)$ to the spherical coordinate angles β_1 and β_2 which locate the observation point with respect to the z_1 and z_2 axes, respectively (see Fig. 1).

The critical points in i) and ii) play a different role in the asymptotic evaluation of the integral in (3) with respect to their dependence on the observer location. For observation points close to the array surface and far from the array edges and vertexes, the oscillations of the individual element spec-

tral GF are rather slow; therefore, the periodic, highly peaked spectral function $I_1(k_{z_1})I_2(k_{z_2})$ acts like a passband periodic filter for that GF. As shall be demonstrated in the next section, the outcome of this sampling is the FW summation corresponding to the infinite array, with adiabatic modulation due to the tapering function. When the observation point is in the far zone of the array (i.e., at distance greater than $2D^2/\lambda$), the oscillations around the stationary phase point are so rapid as to localize the contributions from the periodic function $I_1(k_{z_1})I_2(k_{z_2})$ to its values at $(\bar{k}^s_{z_1}, \bar{k}^s_{z_2})$. Consequently, the far field is proportional to $I_1(\bar{k}^s_{z_1})I_2(\bar{k}^s_{z_2})$. The recognition that this expression is the ordinary "array factor" associated with the pattern multiplication law [12] has motivated our designation of $I_1(k_{z_1})I_2(k_{z_2})$ as the *spectral array factor*.

In the intermediate zone (Fresnel zone) where the distance of the observation point from the array and the size of the array may be comparable, both types of critical points and their interaction have to be taken into account in the asymptotic evaluation of the integral. In this intermediate regime, Fig. 2(b) depicts the SAF in one periodicity cell, and Fig. 2(c) displays the corresponding phase modulation associated with the GF. The two plots exhibit comparable variation, and it is not evident how to identify a spectral filtering that quantifies the influence of one factor on the other. We therefore refine the asymptotics and introduce *additional* critical points to account for *transitions* between the various wave types.

iii) $(k_{z_1}, k_{z_2}) = (k^s_{z_1}, k_{z_{2,p}})$ and $(k_{z_1}, k_{z_2}) = (k_{z_{1,q}}, k^s_{z_2})$. These points satisfy the one-variable stationary phase conditions $(d/dk_{z_1})P(k_{z_1}, k_{z_{2,p}}) = 0$ and $(d/dk_{z_2})P(k_{z_{1,q}}, k_{z_2}) = 0$ respectively, with $P(k_{z_1}, k_{z_2}) = k_{z_1}z_1 + k_{z_2}z_2 + k_y y$. The asymptotic wavefields corresponding to these two saddle points tag diffracted fields from edge 2 (located at $z_1 = 0$) and edge 1 (at $z_2 = 0$), respectively. For a rectangular array, diffraction from the other two edges can be found similarly by including the appropriate phase reference in the second term on the right-hand side of (5).

The asymptotic contributions pertaining to the three types of critical points are examined next. Though the critical points are the same as those in [3], the localization process is conducted differently here by introducing the *quasi-poles* and a spatial-spectral expansion [see (17) and (36)] of the spectral integrand in (3) for the end-point evaluations (edge- and vertex-diffracted waves).

IV. Uniform High-Frequency Solutions

Because of the slowly varying assumption for the tapering function $f_i(z_i)$, adiabatic methods can be applied, based on perturbation about $f_i(z_i) =$const. The case of equiamplitude excitation, which has been treated in [3] and [4], is briefly summarized here for convenience.

A. Equiamplitude Excitation $f_i = 1$

1) *Finite array:* Since $f_i = 1$, the series $I_i(k_{z_i})$ in (4) can be evaluated in closed form: $I_i(k_{z_i}) = B_i(k_{z_i})(1 - e^{jN_i d_i(k_{z_i} - \gamma_i)}), i = 1, 2$; here, $B_i(k_{z_i})$ exhibits singularities at $k_{z_i} = k_{z_{i,u}}$ that are cancelled by the zeros of the numerator in $I_i(k_{z_i})$ (see Fig. 2). Because the functions $I_i(k_{z_i})$ are recognized as the analytic continuation of the spectral array factor in the complex k_{z_i}-plane, the SAF exhibits peaks at the values $k_{z_i} = k_{z_{i,u}}$, i.e., at the FW wavenumbers in (7).

2) *Infinite array:* When the number of array elements in both dimensions increases, the peaks of the SAF become correspondingly enhanced and, in the limit of an infinite number of dipoles, tend to two separate sequences of Dirac delta functions

$$I_i(k_{z_i}) \to \sum_{s=-\infty}^{\infty} e^{j(k_{z_i} - \gamma_i)sd_i} = \frac{2\pi}{d_i} \sum_{u=-\infty}^{\infty} \delta\left(k_{z_i} - k_{z_{i,u}}\right) \tag{8}$$

with $\mathrm{i} = 1, 2$. This reduces the integral in (3) to the periodicity-modulated FW series for the infinite AGF

$$A_\infty(\mathbf{r}) = \sum_{p,q=-\infty}^{\infty} A^{\mathrm{FW}}_{pq}; \quad A^{\mathrm{FW}}_{pq} = \frac{e^{-j\mathbf{k}^{\mathrm{FW}}_{pq}\cdot\mathbf{r}}}{2jd_1d_2k_{y_{pq}}} \tag{9}$$

where $\mathbf{k}^{\mathrm{FW}}_{pq} = k_{z_{1,q}}\hat{\mathbf{z}}_1 + k_{z_{2,p}}\hat{\mathbf{z}}_2 + k_{y_{pq}}\hat{\mathbf{y}}, k_{y_{pq}} = \sqrt{k^2 - k^2_{z_{1,q}} - k^2_{z_{2,p}}}$.

3) *Planar sectoral array:* When the upper limit N_i in the series (4) is extended to infinity one obtains (assuming small losses), $I_i(k_{z_i}) \to B_i(k_{z_i})$. For this case, the asymptotic evaluation of (3) can be performed as in [3] via sequential deformation of the original double integration contour into the complex k_{z_2}-plane local steepest descent path (SDP) along the 45° line through the saddle point of the phase in the integrand, with extraction of the residues at intercepted poles. These residues reconstruct the FW series of the infinite AGF with the proper truncation functions.

B. Weakly Amplitude-Modulated FW Contributions and Shadow Boundary Planes

We begin by assuming that the observer is located far from the array edges in terms of wavelength. Therefore the dominant contributions to the field arise from the peaks associated with the quasi-poles. Generalizing the one-dimensional taper analysis in [5], by inserting (5) into (3), the contributions from the critical points at $(k_{z_1}, k_{z_2}) = (k_{z_{1,q}}, k_{z_{2,p}})$ are found by expanding the exponent $P(k_{z_1}, k_{z_2})$ of the integrand in (3) in Taylor series in a neighborhood of $(k_{z_{1,q}}, k_{z_{2,p}})$

$$P(k_{z_1}, k_{z_2}) \approx \mathbf{k}^{\mathrm{FW}}_{pq}\cdot\mathbf{r} + z_{1pq}\left(k_{z_1} - k_{z_{1,q}}\right) + z_{2pq}\left(k_{z_2} - k_{z_{2,p}}\right) \tag{10}$$

with

$$z_{1pq} = \left.\frac{\partial P\left(k_{z_1}, k_{z_{2,p}}\right)}{\partial k_{z_1}}\right|_{k_{z_1} = k_{z_{1,q}}} = z_1 - y k_{z_{1,q}}/k_{ypq}$$

$$z_{2pq} = \left.\frac{\partial P\left(k_{z_{1,q}}, k_{z_2}\right)}{\partial k_{z_2}}\right|_{k_{z_2} = k_{z_{2,p}}} = z_2 - y k_{z_{2,p}}/k_{ypq}.$$

Next, approximating $k_y^{-1} \approx k_{ypq}^{-1} + k_{z_{1,q}} k_{ypq}^{-3}(k_{z_1} - k_{z_{1,q}}) + k_{z_{2,p}} k_{ypq}^{-3}(k_{z_2} - k_{z_{2,p}})$, and retaining only the dominant asymptotic term of the remainder, one finds $(e^{-jP(k_{z_1},k_{z_2})})/(k_y) \approx (e^{-j\mathbf{k}_{pq}^{\mathrm{FW}}\cdot\mathbf{r}})/(k_{ypq}) e^{-jz_{1pq}(k_{z_1}-k_{z_{1,q}})-jz_{2pq}(k_{z_2}-k_{z_{2,p}})}$ plus higher order terms of type $O(k_{z_1} - k_{z_{1,q}})O(k_{z_2} - k_{z_{2,p}})$. Here, $k_{ypq} = \sqrt{k^2 - k_{z_{1,q}}^2 - k_{z_{2,p}}^2}$, with the branches chosen as for k_y (see Section III-A), is real for propagating FW. Inserting (10) into (3) [and approximating the slowly varying portion of the integrand by its value at $(k_{z_{1,q}}, k_{z_{2,p}})$], leads to

$$A^{\mathrm{FW}}(\mathbf{r}) \approx \frac{1}{4\pi^2} \sum_{p,q=-\infty}^{\infty} \Bigg[A_{pq}^{\mathrm{FW}}(\mathbf{r}) \cdot \prod_{i=1,2} \int_{-\infty}^{\infty} \tilde{f}_i\left(k_{z_i} - k_{z_{i,u}}\right) \cdot e^{-jz_{ipq}\left(k_{z_i} - k_{z_{i,u}}\right)}\, dk_{z_i} \Bigg]. \quad (11)$$

The two spectral integrals are calculated directly, using the definition in (6), yielding

$$A^{\mathrm{FW}}(\mathbf{r}) \approx \sum_{p,q=-\infty}^{\infty} A_{pq}^{\mathrm{FW}}(\mathbf{r}) f_1(z_{1pq}) f_2(z_{2pq}). \quad (12)$$

In (11) and (12), $A_{pq}^{\mathrm{FW}}(\mathbf{r})$ is the pqth FW for equiamplitude excitation [see (9)], which is multiplied in (12) by the tapering function $f_1(z_{1pq})f_2(z_{2pq})$ evaluated at the footprint (z_{1pq}, z_{2pq}) of the pqth FW. Note that the two vertex-truncation terms in (5), $(f_i(0))/(2)$ and $(f_i(L_i))/(2)e^{j(k_{z_i}-\gamma_i)L_i}$, for both $i = 1, 2$, are not included here because they provide additional contributions from edge and vertex diffractions, which are calculated separately using (10).

The stationary phase evaluation of the *Kirchhoff spatial* radiation integral associated with each pqth equivalent FW-matched aperture distribution would provide the same result as in (12) since (z_{1pq}, z_{2pq}) is the corresponding *space domain* stationary phase point. We note that since $f_i(z_{ipq}) = 0$ for $z_i < 0, z_i > L_i$, the tapering function automatically truncates the FW domain of existence at the shadow boundary (SB) planes defined by the conditions $z_{1pq} = 0$ and $z_{2pq} = 0$, which correspond to $(z_1/y) = (k_{z_{1,q}})/(k_{ypq})$ and $(z_2/y) = (k_{z_{2,p}})/(k_{ypq})$, respectively. In the angular space domain, these two conditions become $\phi_1 = \phi_{1,pq}^{\mathrm{SB}}$ and $\phi_2 = \phi_{2,pq}^{\mathrm{SB}}$, where ϕ_i is the transverse-to-z_i observation angle (see Figs. 1 and 3) and

$$\phi_{1,pq}^{\mathrm{SB}} = \cos^{-1}\left(k_{z_{2,p}}/k_{\rho_{1,q}}\right)$$
$$\phi_{2,pq}^{\mathrm{SB}} = \cos^{-1}\left(k_{z_{1,q}}/k_{\rho_{2,p}}\right). \quad (13)$$

Here, $k_{\rho_{1,q}} = \sqrt{k^2 - k_{z_{1,q}}^2}$ and $k_{\rho_{2,p}} = \sqrt{k^2 - k_{z_{2,p}}^2}$ define the shadow boundary planes (SBPs) associated with the two edges that intersect at the vertex $(z_1, z_2) = (0, 0)$; in Fig. 3, these SBPs are displayed for two edges of the rectangular array.

C. FW-Induced Amplitude-Modulated Diffracted Fields and Shadow Boundary Cones

As noted in Section III-B, the critical points ii) give rise to edge-diffracted field contributions from the four edges of the rectangular array. The procedure to obtain these contributions is based on that presented in [5] and is summarized in Appendix I.

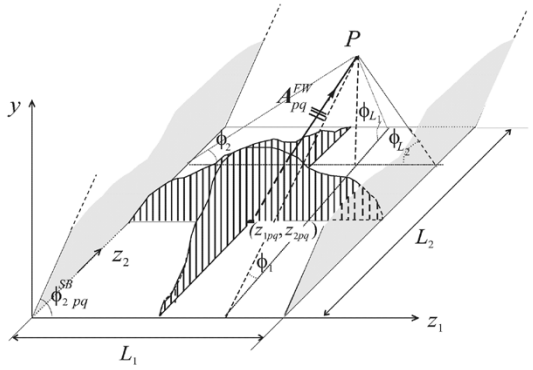

Fig. 3. (p, q)th FW shadow boundaries for rectangular array. The (p, q)th propagating FW exists inside the four (p, q)th shadow boundaries (SBs), originating at the point $(z_{1pq}, z_{2pq}) = (z_1 - yk_{z_1,q}/k_{ypq}, z_2 - yk_{z_2,p}/k_{ypq})$. The shadow boundary planes relevant to edge 1 and 2 are defined by $\phi_1 = \phi_{1,pq}^{\mathrm{SB}}$, and $\phi_2 = \phi_{2,pq}^{\mathrm{SB}}$ in (13), respectively.

Denoting by $f_2'(z_2)$ and $B_2'(k_{z_2})$ the derivative of $f_2(z_2)$ and $B_2(k_{z_2})$ with respect to their arguments, the diffracted field from edge 1 is given by

$$A_q^{d,1}(\mathbf{r}) \sim \frac{f_1\left(z_{1q}^{d,1}\right) e^{-j\mathbf{k}_q^{d,1}\cdot\mathbf{r}}}{2d_1\sqrt{2\pi j\rho_1 k_{\rho_{1,q}}}} \cdot \left[f_2(0) B_2\left(k_{z_2}^s\right) F\left(\delta_{1,pq}^2\right) - j f_2'(0) B_2'\left(k_{z_2}^s\right) F_s\left(\delta_{1,pq}^2\right) \right] \quad (14)$$

where the amplitude tapering function f_1 in the $z_1$direction is evaluated at the footprint of the qth edge-diffracted field along edge 1 : $z_{1,q}^{d,1} = z_1 - \rho_1 k_{z_{1,q}}/k_{\rho_{1,q}}$. Since $f_1(z_{1,q}^{d,1}) = 0$ for $z_{1q}^{d,1} < 0$ and $z_{1,q}^{d,1} > L_1$, the domain of existence of the qth edge-diffracted field is bounded automatically. The truncation at $z_{1q}^{d,1} = 0$ corresponds to $(z_1/\rho_1) = (k_{z_{1,q}})/(k_{\rho_{1,q}})$, which becomes in the angular space domain $\beta_1 = \beta_{1q}^{\mathrm{SB}} = \cos^{-1}(k_{z_{1,q}}/k)$, where β_1 is the conical angle (see Fig. 1). Equation $\beta_1 = \beta_{1,q}^{\mathrm{SB}}$ characterizes the shadow boundary cone ($\mathrm{SBC}_{1,q}$) which, centered at the vertex (Fig. 4), confines the diffracted field. The $\mathrm{SBC}_{1,q}$, centered at the vertex (Fig. 4), has the same aperture as the diffraction cone [analogous considerations apply to the p-indexed q independent z_2-edge diffracted rays, whose domain of existence is confined by $U(\beta_{2,p}^{\mathrm{SB}} - \beta_2)$], where U is the Heaviside unit step functions. In (14), $\mathbf{k}_q^{d,1} = k_{z_{1,q}}\hat{\mathbf{z}}_1 + k_{\rho_{1,q}}\cos\phi_1\hat{\mathbf{z}}_2 + k_{\rho_{1,q}}\sin\phi_1\hat{\mathbf{y}}$ denotes the vector wavenumber of the qth diffracted field, and lies on the surface of a diffraction cone centered at $z_{1,q}^{d,1}$ on the array edge, forming an angle $\beta_{1,q}^{\mathrm{SB}}$ with the z_1-axis. Moreover, $F(x)$ in (14) is the standard uniform theory of diffraction (UTD) transition function [13]

$$F(x) = 2j\sqrt{x}e^{jx}\int_{\sqrt{x}}^{\infty} e^{-jt^2}\, dt, \quad -\frac{3\pi}{2} < \arg(x) < \frac{\pi}{2} \quad (15)$$

$$F_s(x) = 2jx[1 - F(x)] \quad (16)$$

is the slope UTD transition function (see Appendix I and [14]). It can be shown that when the nondimensional parameter $\delta_{1,pq}^2 = 2k_{\rho_{1,q}}\rho_1\sin^2((1/2)(\phi_{1pq}^{\mathrm{SB}} - \phi_1))$ is large, F and F_s both tend to unity.

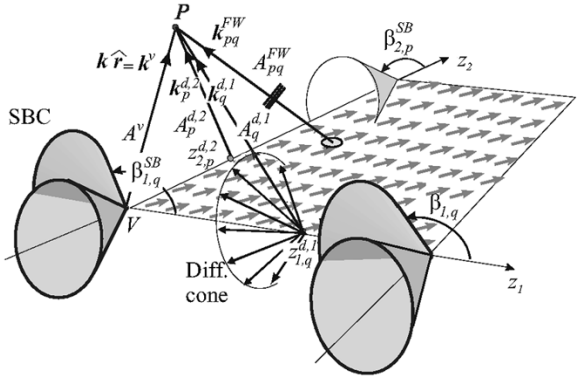

Fig. 4. Ray description of the field radiated by the rectangular array of dipoles. The diffraction cone of the propagating z_1-edge (z_2-edge) diffracted ray originates at the q-dependent (p-dependent) point $z_{1,q}^{d,1}$ on edge 1 ($z_{2,p}^{d,2}$ on edge 2). The SBC that truncates the domain of existence of the qth edge diffracted field has the same aperture angle $\beta_{1,q}$ as the diffraction cone and is centered at the vertex. The diffracted rays from edges 1 and 2 are associated with the wavevectors $\mathbf{k}_q^{d,1} = \hat{\mathbf{z}}_1 k_{z_1,q} + \hat{\mathbf{z}}_2 k_{\rho_1,q}\cos\phi_1 + \hat{\mathbf{y}} k_{\rho_1,q}\sin\phi_1$ and $\mathbf{k}_p^{d,2} = \hat{\mathbf{z}}_2 k_{z_2,p} + \hat{\mathbf{z}}_1 k_{\rho_2,p}\cos\phi_2 + \hat{\mathbf{y}} k_{\rho_2,p}\sin\phi_2$, respectively. These rays are truncated at the SBCs $\beta_1 = \beta_{1,q}$ and $\beta_2 = \beta_{2,p}$ with respect to the axes along edges 1 and 2, respectively. These two SBCs intersect along the intersection line of the two FW-SBs, which coincides with the direction of the propagation vector $\mathbf{k}_{pq}^{\mathrm{FW}} = \hat{\mathbf{z}}_1 k_{z_1,q} + \hat{\mathbf{z}}_2 k_{z_2,p} + \hat{\mathbf{y}} k_{ypq}$ of the pq-FW. The vertex diffracted rays propagate with spherical spreading factor along the wavevector $\mathbf{k}^v = \hat{\mathbf{r}} k$.

The dominant asymptotic term [the first term in (14)] is the same as that for the equiamplitude case (see [2]), except for multiplication by the tapering function evaluated at $z_{1,q}^{d,1}$ on the edge. The second contribution is of higher asymptotic order since $B_2(k_{z_2}) \equiv (1/2) + O(k_{z_2}^{-1})$, whereas $B_2'(k_{z_2}) \equiv O(k_{z_2}^{-2})$. This agrees with the description derived previously for the single tapered edge in [5], as is to be expected in view of the assumptions stated at the beginning of Section IV-B.

The edge diffracted fields from the other edges of the rectangular array have analogous expressions easily deducible from (14).

D. FW-Induced Amplitude Modulated Vertex Diffraction

The critical points iii) in Section III-B parameterize the truncation-induced amplitude modulated vertex-diffracted field effects. These describe truly *new* phenomena that were not encountered in [3]–[5]. For instance, near the vertex at $(z_1, z_2) = (0,0)$, the z_1-edge and z_2-edge FW-shadow boundary transitions interact with the vertex-induced SBCs centered on the z_1-axes and z_2-axes, respectively, due to the truncation of the corresponding edge diffracted fields. The confluence of these four SB transitions near the vertex defines the asymptotics pertaining to vertex diffraction, which is implemented by the following steps. First, I_i in (5) is conveniently expanded in such a way as to highlight the behavior of $f_i(z_i)$ at the truncation $z_i = 0$ as

$$I_i(k_{z_i}) \approx f_i(0) B_i(k_{z_i}) - j f_i'(0) B_i'(k_{z_i}) + O\left(\left(k_{z_i} - k_{z_{i,u}}\right)^{-3}\right) \quad (17)$$

where $B_i(k_{z_i})$ is defined in Section IV-A (finite array) and $B_i'(k_{z_i})$ is its derivative (the derivation of (17) is the same as that shown for $I_2(k_{z_2})$ in (33)–(36) of Appendix I). Note that, due to the local approximation (17), pole singularities not present

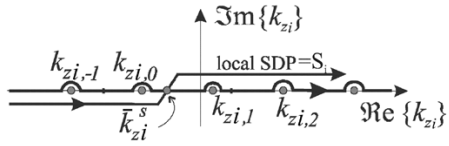

Fig. 5. Topology of the k_{z_i} complex planes. The original integration paths of (3) are along the real axis with clockwise indentation around the poles. As described in Section IV-D and in [3], the original integration paths are deformed locally along the 45°-line SDPs.

in (3) are now introduced. In the following, physical residue contributions associated with these poles are not accounted for here since they represent the physical FW and edge-diffracted fields already discussed in Section IV-C and -B. The presence of the pole singularities allows us to describe the diffraction mechanism by (poles)-(saddle point) interaction implemented through operations on the already developed canonical integral in [3]. From now on, the topology of the spectral plane k_{z_i} is analogous to that treated in [3] for the uniform *sectoral* AGF.

Insertion of the asymptotic expansion (17) of $I_i(k_{z_i})$ into (3) permits the diffracted field from vertex $(z_1, z_2) = (0,0)$ to be expressed as a sum of four terms

$$A^{v,1}(\mathbf{r}) \sim \sum_{h=1}^{4} A_h^{v,1}(\mathbf{r}) \quad (18)$$

with

$$A_h^{v,1}(\mathbf{r}) = \frac{f_1^{(m)}(0) f_2^{(l)}(0)}{8\pi^2 j^{m+l+1}} \cdot \int_{S_i}\int_{S_i} \frac{e^{-jP(k_{z_1},k_{z_2})}}{k_y} B_1^{(m)}(k_{z_1}) B_2^{(l)}(k_{z_2})\, dk_{z_1} dk_{z_2} \quad (19)$$

where S_i are the local SDPs in the plane k_{z_i}. The superscript $^{(\alpha)}$ denotes the αth derivative; for $h = 1 : m = l = 0$; for $h = 2 : m = 0, l = 1$; for $h = 3 : m = 1, l = 0$; and for $h = 4 : m = l = 1$. The integration paths in (19) are along the local-SDP for each variable k_{z_i}, as shown in Fig. 5, intercepting the real axis at the saddle point (SP) $\bar{k}_{z_i}^s$.

The double integral (19) for the case $m = l = 0$ was evaluated in [3], with details given of the path deformations in both variables. The regularization process in that case involves the Van der Waerden (VdW) method, which uses selective *addition* and *subtraction* of pole singularities. We have also suggested in [3] the use of the Pauli–Clemmow method [15] because it incorporates the relevant phenomenologies in a simpler format than the VdW method. In particular the Pauli–Clemmow method involves selective *multiplication* and *division* by the regularizing functions $W_{1,q} = [-jd_1(k_{z_1} - k_{z_{1,q}})]^{-1}, W_{2,p} = [-jd_2(k_{z_2} - k_{z_{2,p}})]^{-1}, \partial W_{1,q}/\partial k_{z_1} = [jd_1(k_{z_1} - k_{z_{1,q}})^2]^{-1}, \partial W_{2,p}/\partial k_{z_2} = [jd_2(k_{z_2} - k_{z_{2,p}})^2]^{-1}$. In this paper we extend the Pauli–Clemmow method to accommodate "slope diffraction effects." For simplicity, we develop expressions only for regularization of the (p,q) pole which is closest to the SP. For the vertex problem, the critical parameters are tied to the $(k_{z_1}, k_{z_2}) = (\bar{k}_{z_1}^s, \bar{k}_{z_2}^s) = (k\cos\beta_1, k\cos\beta_2)$ first-order SP, and to the k_{z_1}- and k_{z_2}-poles in (3), i.e., (p,q) that minimize the spectral distances $|\bar{k}_{z_1}^s - k_{z_{1,q}}| = k|\cos\beta_1 - \cos\beta_{1,q}|$ and $|\bar{k}_{z_2}^s - k_{z_{2,p}}| = k|\cos\beta_2 - \cos\beta_{2,p}|$. For details see [3] and

TABLE I
ASYMPTOTIC BEHAVIOR OF THE TRANSITION FUNCTIONS $T_h(a,b,w)$ FOR LARGE VALUES OF a AND/OR b. THE PARAMETERS a (b) ARE LARGE WHEN THE OBSERVER IS "FAR" FROM $\mathrm{SBC}_1(\mathrm{SBC}_2)$, OR WHEN THE OPERATING FREQUENCY IS HIGH ENOUGH

	$\|a\|>>1$ $\|b\|>>1$	$\|a\|>>1$	$\|b\|>>1$
$T_1(a,b,w)$	1	$F(b^2)$	$F(a^2)$
$T_2(a,b,w)$	1	$F_s(b^2)$	$F(a^2)$
$T_3(a,b,w)$	1	$F(b^2)$	$F_s(a^2)$
$T_4(a,b,w)$	1	$F_s(b^2)$	$F_s(a^2)$

[16]. The resulting expressions for each h-indexed integral in (19) are

$$A_h^{v,1} \sim \frac{(-j)^{m+l} f_1^{(m)}(0) f_2^{(l)}(0) e^{-jkr}}{4\pi r} \cdot B_1^{(m)}\left(\bar{k}_{z_1}^s\right) B_2^{(l)}\left(\bar{k}_{z_2}^s\right) T_h(a_q, b_p, w) \quad (20)$$

where the locally uniform canonical functions $T_h, h = 1,2,3,4$, are defined as

$$T_h(a_q,b_p,w) = \frac{(-1)^{m+l} a_q^{m+1} b_p^{l+1}}{j\pi(1-w^2)^{\frac{m+l+1}{2}}} \cdot \int_{-\infty}^{\infty}\int_{-\infty}^{\infty} \frac{e^{j(\xi^2+2w\xi\eta+\eta^2)}}{\left(\xi-\frac{a_q}{\sqrt{1-w^2}}\right)^{m+1}\left(\eta-\frac{b_p}{\sqrt{1-w^2}}\right)^{l+1}} d\eta d\xi. \quad (21)$$

The remaining parameters are defined as $a_q = \sqrt{2kr}\sin((\beta_{1,q}-\beta_1)/(2))$, $b_p = \sqrt{2kr}\sin((\beta_{2,p}-\beta_2)/(2))$, and $w = \cot\beta_1 \cot\beta_2 = \cos\phi_1\cos\phi_2$, with angles ϕ_1, ϕ_2, and β_1, β_2 defined in Figs. 1 and 3, and SB angles $\beta_{1,q}, \beta_{2,p}$ defined after (14) and in Fig. 4 (see [3] for details). Results obtained from (20) are comparable to those obtained applying the VdW procedure in a region "not too close" to the vertex $(z_1, z_2) = (0,0)$ of the array. Again, as in [3], approaching the vertex, the diffraction coefficient due to the VdW is superior; however, when the Pauli–Clemmow evaluation is augmented with the "slope" diffraction term, (20) and the *globally regularized* version of the VdW perform comparably. For the case of $T_1(a,b,w)$ (nontapered amplitude), the treatment of the vicinity of the vertex has been carried out in [3] and it has been shown that the function $T_1(a,b,w)$, denoted in [3] simply by $T(a,b,w)$, is based on a modification of a less explicit four-parameter function introduced in [17], and thereafter used in [18]. The new remaining $h = 2,3,4$ vertex transition functions are defined by mapping the relevant configurations of critical points in the corresponding original integrals (19) onto the *simplest* canonical integrands. The resulting functions are normalized in such a way as to tend toward unity for large values of a_q, b_p (see Table I). Thus, "far" from the SBCs and the vertex $(z_1, z_2) = (0,0)$ (or, alternatively, for high enough frequencies), the (nonuniform asymptotic) vertex-diffracted field is represented entirely in terms of four spherical wave contributions. "Near" the SBCs (i.e., near the vertex), the locally uniform transition functions $T_h, h = 2,3,4$, differ from unity and can be expressed as combinations of Fresnel integrals and "ordinary" T_1 functions as shown in Appendix II and Section IV-A.

V. TOTAL ASYMPTOTIC POTENTIAL SYNTHESIS

A. Formal Solution

To synthesize the total high-frequency asymptotic solution for the rectangular array potential, referring to Sections IV-A–D, we obtain

$$A^{\mathrm{tot}}(\mathbf{r}) = \sum_{p,q} A_{pq}^{\mathrm{FW}}(\mathbf{r}) f_1(z_{1pq}) f_2(z_{2pq}) + \sum_q \left(A_q^{d,1}(\mathbf{r}) + A_q^{d,3}(\mathbf{r})\right) + \sum_p \left(A_p^{d,2}(\mathbf{r}) + A_p^{d,4}(\mathbf{r})\right) + \sum_{i=1}^{4}\sum_{h=1}^{4} A_h^{v,i}(\mathbf{r}). \quad (22)$$

Note that the domains of existence of the various wave species are automatically embedded in the definitions of $f_i(z_i)$ inside the expressions of the FWs in (12) and of the diffracted fields in (14). The domains of existence of the FWs and diffracted fields are given in terms of $f_i(z_i)$ and the SB planes and cones in the text in connection with (12) and (14), respectively (see Figs. 3 and 4).

B. Transition Functions

Since the numerical evaluation of T_1 in (21) can be performed efficiently as in [16], [19], and [20] in terms of standard generalized Fresnel integrals [20], it is convenient to numerically evaluate $T_h, h = 2,3,4$ in (21) in terms of the function T_1 and the UTD transition functions F and F_s. In Appendix II, the transition functions $T_h, h = 2,3,4$, in (21) have been expressed exactly in terms of the function $T = T_1, F(x)$ and $F_s(x)$ as follows:

$$T_2(a,b,w) = \frac{2jb}{1-w^2}\cdot[bF(a^2) - b + waT_1(a,b,w) + waF(b^2)] \quad (23)$$

$$T_4(a,b,w) = \frac{2jb}{1-w^2}\cdot[bF_S(a^2) - b + waT_3(a,b,w) + waT_1(a,b,w)] \quad (24)$$

and $T_3(a,b,w) = T_2(b,a,w)$, where F and F_s are defined in (15) and (16), respectively.

For simplicity of notation, we discuss the asymptotic order estimates and field behavior associated with vertex $(z_1, z_2) = (0,0)$. For the other vertexes the same rules apply in their respective local coordinates. The vertex-diffracted field $A^{v,1}(\mathbf{r})$ [associated with $(z_1, z_2) = (0,0)$] incorporates the transition from a vertex-dominated spherical wave to an edge-dominated cylindrical wave and it compensates for the discontinuities (across the SBCs) of the edge-diffracted rays at $\beta_1 = \beta_{1,q}$ and $\beta_2 = \beta_{2,p}$ (see Fig. 4); the respective approximate parameters a_q, b_p vanish there. The asymptotically dominant terms in the compensation mechanism at $\beta_1 = \beta_{1,q}$ are those involving $F(a_q^2)$ and $T_1(a_q, b_p, w)$, with the latter behaving like $F(a_q^2)$ for β_2 significantly distinct from $\beta_{2,p}$. Analogous considerations apply for $\beta_2 = \beta_{2,p}$. At the simultaneous intersection of the conical $\mathrm{SBC}_{1,2}$ and the truncated FW planar $\mathrm{SB}_{1,2}$, both a_q and b_p vanish (see [3, Fig. 3]), and the corresponding $T_1(a_q, b_p, w)$ function transforms the vertex-induced field locally into a *plane wave* to match the FW.

TABLE II
DIFFRACTION AND COMPENSATION MECHANISMS. COLUMN 1 (WAVE SPECIES): FLOQUET WAVES, FW$_{pq}$; DIFFRACTED WAVES AT EDGE i, Ei; SLOPE-DIFFRACTED WAVES AT EDGE i, EiS; DIFFRACTED WAVES AT VERTEX 1, V; SLOPE-DIFFRACTED WAVES AT VERTEX 1, 2, VS$i,j$; DOUBLE SLOPE-DIFFRACTED WAVES AT VERTEX 1, VSS. COLUMN 2: SPREADING FACTOR. COLUMN 3: WAVE SPECIES AMPLITUDES. NOTATION $B_i^{(\alpha)}$ CORRESPONDS TO $B_i^{(\alpha)}(k_{z_i}^s), i = 1, 2$. COLUMN 4: COMPENSATION MECHANISMS

Wave Species	*Spreading Factor*	*Complex Amplitude*	*Compensation Mechanisms*
FW	1	$f_1(z_{1pq})f_2(z_{1pq})$	
E1	$1/\sqrt{\rho_1}$	$f_1(z_{1q}^{d,1})f_2(0)B_2F(\delta_{1,pq}^2)$	ϕ_1=$\phi_{1,pq}^{SB}$ $\rightarrow$ FW
E1S	$1/\sqrt{\rho_1}$	$jf_1(z_{1q}^{d,1})f_2^{'}(0)B_2^{'}F_s(\delta_{1,pq}^2)$	
E2	$1/\sqrt{\rho_2}$	$f_2(z_{2p}^{d,2})f_1(0)B_1F(\delta_{2,pq}^2)$	ϕ_2=$\phi_{2,pq}^{SB}$ $\rightarrow$ FW
E2S	$1/\sqrt{\rho_2}$	$jf_2(z_{2p}^{d,2})f_1^{'}(0)B_1^{'}F_s(\delta_{2,pq}^2)$	
V	$1/r$	$f_1(0)f_2(0)B_1B_2T$	β_1=$\beta_{1,q}^{SB}$ $\rightarrow$ E1 β_2=$\beta_{2,p}^{SB}$ $\rightarrow$ E2
VS1	$1/r$	$jf_1^{'}(0)f_2(0)B_1^{'}B_2T_2$	β_2=$\beta_{2,p}^{SB}$ $\rightarrow$ E2S
VS2	$1/r$	$jf_1(0)f_2^{'}(0)B_1B_2^{'}T_3$	β_1=$\beta_{1,q}^{SB}$ $\rightarrow$ E1S
VSS	$1/r$	$-f_1{'}(0)f_2^{'}(0)B_1{'}B_2^{'}T_4$	

The transitional behavior of the other vertex diffracted transition functions $T_h, h = 1,2,3,4$ is summarized in Table I. The functions T_h tend toward unity for large values of a_q and b_p. Large values of *both* a_q and b_p imply significant spectral domain plane separation between the poles and the SP, and define the nonuniform ray regime. When only *one* of the parameters a_q or b_p is large, only *one* of the two poles is asymptotically far away from the SP, and T_1 yields the canonical UTD transition function. The limit for $b_p \gg 1$ can be obtained directly from (21) on approximating the denominator in the integrand by its value at $\eta = 0$ [i.e., $(\eta - b_p/\sqrt{1-w^2})^{-1} \approx -b_p^{-1}\sqrt{1-w^2}$] and recognizing the remaining single-pole integral as the ordinary one-parameter UTD transition function $F(a_q^2)$. Concerning the functions T_2 and T_3 in (21), the large parameter a_q (or b_p) range is characterized by a double-pole integral that can be expressed in terms of the UTD slope transition function $F_s(x)$ (see Table I).

The vertex-diffracted contribution $A_1^{v,1}$ containing T_1 accounts for the transition from a vertex-centered spherical wave to an edge-centered cylindrical wave and it compensates for the discontinuities across the relevant SBCs (see [3]). The other vertex diffracted terms $A_h^{v,1}, h = 2,3,4$, not present in [3], are of higher asymptotic order and compensate for the discontinuities across the SBCs of the diffracted wave associated with the derivative of the tapering functions at the edges. Note that when the excitation function tends to zero at the vertex from both directions z_1 and z_2, only the contribution $A_4^{v,1}$ remains. The various compensation mechanisms are summarized in Table II. The spreading factors and complex amplitudes are shown for each field contribution associated with vertex $(z_1, z_2) = (0,0)$, namely, $A_{pq}^{\mathrm{FW}}, A_q^{d,1}, A_p^{d,2}$, and $A^{v,1}$. As shown in the last column, diffracted field species reduce to other wave species at the planar and conical SBs.

VI. TOTAL VECTOR ELECTRIC FIELD SYNTHESIS

The electric vector fields are obtained from the vector potential $\mathbf{A} = A\hat{\mathbf{J}}_0$ via $\mathbf{E} = -j\omega\mu(\mathbf{A}+\nabla\nabla\cdot\mathbf{A}/k^2)$ and $\mathbf{H} = \nabla\times\mathbf{A}$. When the differential operators are applied to the spectral representation (3), interchanging the order of integration and differentiation yields (noting that $\nabla \rightarrow -j\mathbf{k}$ in the spectral domain)

$$\mathbf{E}(\mathbf{r}) = \frac{1}{8\pi^2}\int_{-\infty}^{\infty}\int_{-\infty}^{\infty}\frac{I_1(k_{z_1})\,I_2(k_{z_2})}{k_y}\bar{\bar{\mathbf{G}}}^E(\mathbf{k}) \cdot\hat{\mathbf{J}}_0 e^{-j\mathbf{k}\cdot\mathbf{r}}\,dk_{z_1}dk_{z_2} \quad (25)$$

where $\bar{\bar{\mathbf{G}}}^E(\mathbf{k}) = -\zeta/k(k^2\bar{\bar{\mathbf{I}}} - \mathbf{kk})$, $\bar{\bar{\mathbf{I}}}$ denotes the unit dyadic, ζ is the free space impedance and the notation $\mathbf{k}$ in $\bar{\bar{\mathbf{G}}}^E(\mathbf{k})$ implies a dependence on $(k_{z_1}, k_{z_2}, k_y(k_{z_1}, k_{z_2}))$. The magnetic field is treated formally in similar fashion, leading to the replacement of $\bar{\bar{\mathbf{G}}}^E(\mathbf{k})$ by the magnetic dyadic $\bar{\bar{\mathbf{G}}}^H(\mathbf{k}) = -\mathbf{k}\times\bar{\bar{\mathbf{I}}}$. The asymptotic evaluation of (25) is carried out in the same manner as for the potential A in (3), except that we now take into account the extra term $\bar{\bar{\mathbf{G}}}^E(\mathbf{k})$. The integral in (25) is dominated asymptotically by the same critical spectral points as in Section III-B, whence the evaluation procedure is the same as in Sections II–IV.

The polarization dyadic $\bar{\bar{\mathbf{G}}}^E(\mathbf{k})$ may be assumed to be slowly varying so that (25) can be evaluated by the procedure used in Section IV, where the extra term $\bar{\bar{\mathbf{G}}}^E(\mathbf{k})$ is approximated by its value at the critical spectral points

$$\begin{aligned}\mathbf{E}(\mathbf{r}) = &\sum_{p,q}\mathbf{E}_{pq}^{\mathrm{FW}}(\mathbf{r})f_1(z_{1pq})f_2(z_{2pq})\\ &+\sum_q\left(\mathbf{E}_q^{d,1}(\mathbf{r})+\mathbf{E}_q^{d,3}(\mathbf{r})\right)\\ &+\sum_p\left(\mathbf{E}_p^{d,2}(\mathbf{r})+\mathbf{E}_p^{d,4}(\mathbf{r})\right)\\ &+\sum_{i=1}^{4}\sum_{h=1}^{4}\mathbf{E}_h^{v,i}(\mathbf{r}) \end{aligned} \quad (26)$$

with

$$\mathbf{E}_{pq}^{\mathrm{FW}}(\mathbf{r}) = A_{pq}^{\mathrm{FW}}(\mathbf{r})\bar{\bar{\mathbf{G}}}^E\left(\mathbf{k}_{pq}^{\mathrm{FW}}\right)\cdot\hat{\mathbf{J}}_0 \quad (27)$$

$$\mathbf{E}_u^{d,i}(\mathbf{r}) = A_u^{d,i}(\mathbf{r})\bar{\bar{\mathbf{G}}}^E\left(\mathbf{k}_u^{d,i}\right)\cdot\hat{\mathbf{J}}_0 \quad (28)$$

$$\mathbf{E}^{v,i}(\mathbf{r}) = \sum_{h=1}^{4}A_h^{v,i}(\mathbf{r})\bar{\bar{\mathbf{G}}}^E(\mathbf{k}^v)\cdot\hat{\mathbf{J}}_0 \quad (29)$$

in which the wavevectors $\mathbf{k}_{pq}^{\mathrm{FW}}, \mathbf{k}_q^{d,1}, \mathbf{k}_p^{d,2}$, and $\mathbf{k}^v$ are defined in Fig. 4. Similar expressions hold for the other field contributions, which can be expressed conveniently in their ray-fixed reference systems. The reader is referred to [1], [2], and [3] for more details about the asymptotic pertaining to the vector fields.

VII. Numerical Results

Numerical tests have been performed on a "large" square array of dipoles in order to validate the high frequency formulation in (26). An element-by-element summation over the radiated contributions from each dipole serves as a reference. From a variety of near-field scans carried out for different array parameters and dipole orientations, we have selected only some of the most challenging examples because of space limitations. The quality of the analytic-numerical comparisons in the examples is typical of what we have found throughout. The 30×30 element test array of dipoles oriented along $\hat{\mathbf{J}}_0 = \hat{\mathbf{z}}_1$ with identical (z_1, z_2) periods $d_1 = d_2 = 0.5\lambda, \lambda = 2\pi/k$ but with different (z_1, z_2) excitations, is shown in the insets of Fig. 6. Only one propagating FW is excited due to the small array period. Consequently, the total propagating contributions are one truncated FW, four truncated edge-diffracted rays, and four vertex-diffracted rays. The electric field component E_{z_1} observed at a distance $R = 12\lambda$ in the diagonal scan plane depicted in the insets, is shown in Fig. 6, for three different coordinate-separable excitations. In Fig. 6(a), the interelement phasings are $\gamma_1 = \gamma_2 = 0$ (broadside radiation, i.e., main beam at $\theta = 0^\circ$) with excitation function given by a Taylor tapering [27] (SLL$= -25$ dB; the Taylor weights from the edge to the center in both directions are $f_1(n_1 d_1) = f_2(n_2 d_2) = 0.399, 0.407, 0.42, 0.46, 0.51, 0.58, 0.65, 0.73, 0.799, 0.85, 0.9, 0.94, 0.97, 0.99, 1.0$ for $1 \leq n_i \leq 15$ with the remaining weights $(16 \leq n_i \leq 30)$ constructed by symmetry). In Fig. 6(b), the interelement phasings are $\gamma_1 = 0, \gamma_2 = 1.1/\lambda$, yielding a radiated main beam at $\theta = 10^\circ$ with respect to the normal to the array plane, and at $\beta_1 = 90^\circ, \beta_2 = 80^\circ$ with respect to both the z_1 and z_2 axes with tapered excitation functions $f(z_1, z_2) = f_1(z_1) f_2(z_2)$, where $f_i(z_i) = \exp[-((z_i - L_i/2)^2)/(2\sigma^2)]\sigma^2 = L_i^2/(8\ln(c))(c = 0.3)$. In Fig. 6(c), the interelement phasing is $\gamma_1 = \gamma_2 = 2.2/\lambda$, yielding a radiated main beam at $\theta = 30^\circ$ with respect to the normal to the array plane, and at $\beta_1 = \beta_2 = 69^\circ$ with respect to both the z_1 and z_2 axes. The tapering function here is $f_i(z_i) = \sin(\pi z_i / L_i)$. In all three cases, solid curves denote the uniform asymptotic expression for the total radiated field in (26), while dashed curves denote the radiated field in (26) without the vertex contributions. Clearly, the vertex-diffracted waves compensate for the disappearence of the edge-diffracted waves at their SBCs, rendering the total radiated field (solid curves) continuous. The agreement between the asymptotic and numerical reference solutions, which coincide almost everywhere on the scale of the drawing, has been found quite satisfactory even for scan radii smaller than 12λ. Note that the tapered excitation $f_i(z_i) = \sin(\pi z_i / L_i)$ vanishes at the four array edges, i.e., $f_i(0) = f_i(L_i) = 0$. This implies that the four edge-diffracted fields $A_q^{d,i}(\mathbf{r})$ and the four vertex-diffracted fields $A^{v,i}(\mathbf{r}), i = 1, 2, 3, 4$, involve only the slope-diffracted terms $f_i'(0)$, thereby providing a good test case for the usually subdominant additional edge- and vertex-"slope diffracted" contributions. In particular, also in this case, the vertex slope-diffracted fields compensate via the T_4 transition

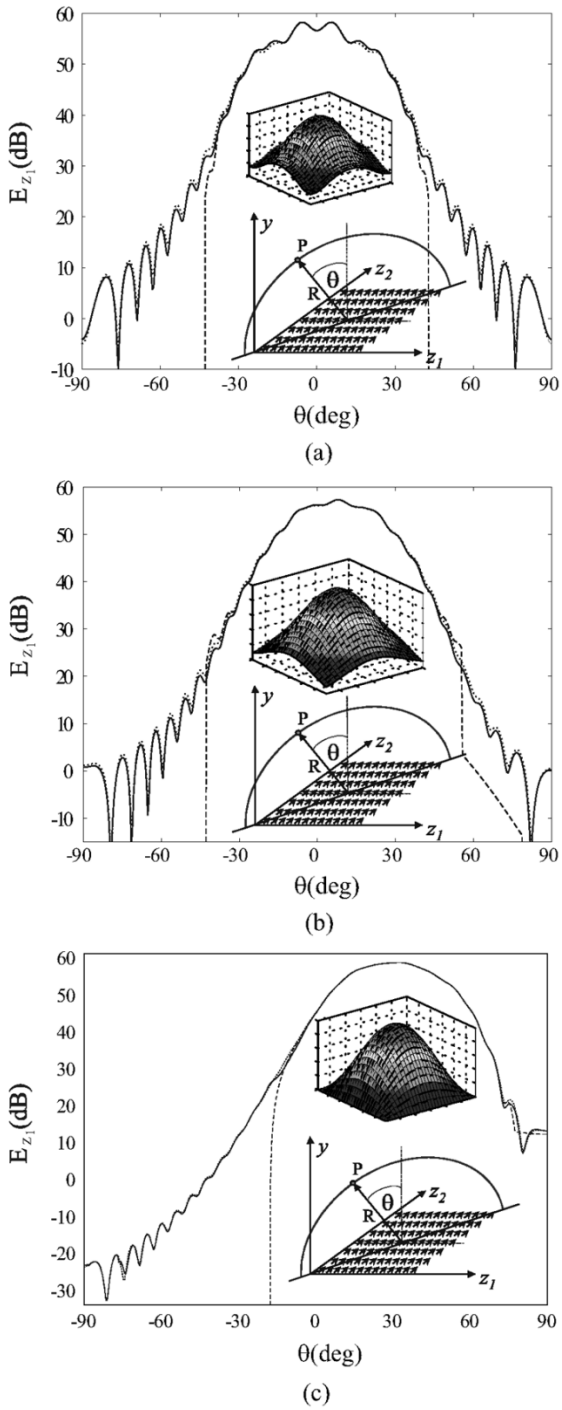

Fig. 6. Electric field radiated by a 30×30 rectangular array of dipoles, with interelement spacings and overall dimensions $L_1 = L_2 = 29 d_1$. Three different excitations are considered: (a) Taylor excitation with $\gamma_1 = \gamma_2 = 0$ (broadside radiation); (b) Gaussian-on-pedestal excitation with $\gamma_1 = 0, \gamma_2 = 1.1/\lambda$; (c) sine excitation with $\gamma_1 = \gamma_2 = 2.2/\lambda$. In all cases, the observation scan at distance $R = 12\lambda$ passes close to two vertexes in a plane normal to the array and tilted 45° from the E plane. Asymptotic solutions from (26) (solid curves), reference solution (dotted curves), and asymptotic solutions without vertex-diffracted fields (dashed curves).

function (last row of Table II) for the disappearance of the edge slope-diffracted fields.

VIII. Conclusion

In this paper, we have analyzed and validated the high-frequency diffraction phenomena pertaining to large rectangular arrays of dipoles with different linear phasings along the two principal coordinates, and with weakly tapered different excitation profiles along these coordinates that may tend to zero at the array edges. The results have been expressed in terms of our previously formulated asymptotic uniformized, periodicity-adapted, FW-modulated GTD for the canonical dipole AGF generated by an infinite plane rectangular sector, which has been generalized here to accommodate the above-mentioned amplitude tapering. The uniform AGF assumes its most intricate form in the vicinity of the vertex, with transition and compensation mechanisms that have been quantified analytically, interpreted phenomenologically, and computed efficiently by our asymptotic algorithm, with accuracy validated through a preliminary set of numerical simulations. The high-frequency results from this analysis can be applied directly to the prediction of the radiation pattern distortion and the interantenna coupling that occurs when the actual array is placed in an electromagnetically complex environment like that of a large array in the antenna farm of a space platform. Such predictions are conventionally obtained by computation-intensive tracing of ray fields from each individual element or a subgroup of elements of the array through the complex environment [7]. Alternatively, global ray tracing based on the direct application of this formulation permits characterization of the entire array aperture radiation in terms of a few rays whose number is independent of the number of array elements, thereby drastically reducing the computational effort. The main effect of the array truncation on the array currents is a global modulation of these currents with a very large period [28], [29]. Although this modulation may perturb the input impedance of the elements, it does not affect significantly the field from the Fresnel zone to the far zone. In other words, the spatial perturbation is filtered by the free-space Green's function (except possibly at grazing aspects). To correctly evaluate this current deformation near the edges of the array, the same FW parametrization of the active array Green's function can be used in a full-wave analysis of the actual rectangular array elements, as demonstrated for short-wire dipoles in [28]–[30] and for open-ended waveguide in an infinite ground plane in [8] and [9].

This paper terminates our long series of investigations of the FW-modulated UTD pertaining to large planar rectangular phased dipole arrays in free space, escalating sequentially from single-edge geometries to two-edge, single-vertex infinite sectors, culminating in the rectangular array. Simultaneously, we have dealt with dipole excitation profiles ranging from equiamplitude through one-dimensional weak tapering to the two-dimensional tapering here. We regard to these studies, in their totality, to have furnished the foundation for the phenomenologically incisive, numerically efficient full-wave treatment of a variety of practical weakly amplitude-tapered phased array antennas (see [12]). While we feel confident that our results so far may be extended to accommodate particular array requirements not covered by weakly tapered or other assumptions, we have initiated the application of these free space algorithms to the important case of dipole arrays printed on, or in, multilayer substrate slabs (see [22]–[24]). However, still ongoing in free space is the separate series of time-domain (TD) canonical studies of sequentially pulsed dipole arrays, which have led to a new FW-modulated TD-UTD [25], [26].

Appendix I
Tapered Edge Diffracted Fields

Here we summarize the procedure for deriving the FW modulated diffracted field at edge 1 (i.e., that at $z_2 = 0$): all other edges may be treated similarly. The relevant critical point is the SPP $k_{z_2}^s$ [see ii) in Section III-B] which satisfies $(d/dk_{z_2})P(k_{z_1,q}, k_{z_2}) = 0$. Inserting (5) into (3), the edge contributions due to the critical point at $(k_{z_1}, k_{z_2}) = (k_{z_1,q}, k_{z_2}^s)$ are found by first expanding the exponent of the integrand in Taylor series around $(k_{z_1,q}, k_{z_2})$, i.e., $P(k_{z_1}, k_{z_2}) \approx \mathbf{k}_q \cdot \mathbf{r} + z_{1,q}(k_{z_1} - k_{z_1,q})$, where $\mathbf{k}_q = k_{z_1,q}\hat{\mathbf{z}}_1 + k_{z_2}\hat{\mathbf{z}}_2 + k_{yq}\hat{\mathbf{y}}$ and $z_{1q} = (\partial P)/(\partial k_{z1})(k_{z_1}, k_{z_2})|_{k_{z_1}=k_{z_1,q}} = z_1 - y k_{z_1,q}/k_{yq}$ and then evaluating $1/k_y$ in a neighborhood of $(k_{z_1,q}, k_{z_2})$. The pertinent asymptotic contribution may be derived from (3) as $A^{d,1}(\mathbf{r}) = \sum_{q=-\infty}^{\infty} A_q^{d,1}$, where

$$A_q^{d,1}(\mathbf{r}) = \int_{-\infty}^{\infty} dk_{z_2} \frac{I_2(k_{z_2})}{8\pi^2 j d_1 k_{yq}} e^{-j\mathbf{k}_q\cdot\mathbf{r}} \cdot \int_{-\infty}^{\infty} \tilde{f}_1\left(k_{z_1} - k_{z_1,q}\right) e^{-jz_{1q}(k_{z_1} - k_{z_1q})}\, dk_{z_1} \quad (30)$$

which, after exact evaluation of the inverse Fourier transform of the integral in k_{z_1}, yields

$$A_q^{d,1}(\mathbf{r}) = \frac{1}{4\pi j d_1} \int_{-\infty}^{\infty} \frac{1}{k_{yq}} I_2(k_{z_2})\, e^{-j\mathbf{k}_q\cdot\mathbf{r}} f_1(z_{1q}(k_{z_2}))\, dk_{z_2}. \quad (31)$$

Note that a) $z_{1q} \equiv z_{1q}(k_{z_2})$ depends on the spectral variable k_{z_2} and b) the two vertex-truncation terms $(f_1(0))/(2)$ and $(f_1(L_1))/(2)e^{j(k_{z_1}-\gamma_1)L_1}$ in (5) are not included in (30), (31) since they will be incorporated subsequently into vertex-diffracted fields to obtain an asymptotic expansion of $I_2(k_{z_2})$ that highlights the behavior of $f_2(z_2)$ at the truncations $z_2 = 0$ and $z_2 = L_2$. The inverse Fourier transform in (6) is approximated asymptotically, using two sequential integrations by parts (we consider only the end-point $z_2 = 0$)

$$\tilde{f}_2\left(k'_{z_2}\right) = \int_0 e^{jk'_{z_2}z_2} f_2(z_2) dz_2 \approx \frac{f_2(0)}{-jk'_{z_2}} + \frac{f_2'(0)}{\left(k'_{z_2}\right)^2}, \quad f'(\xi) = \frac{\partial f}{\partial \xi}. \quad (32)$$

Substituting (32) into (5) and omitting the term $(f_2(L_2))/(2)$ yields

$$I_2(k_{z_2}) = \frac{f_2(0)}{2} + \frac{1}{d_2}\sum_{p=-\infty}^{\infty}\left(\frac{f_2(0)}{-j(k_{z_2}-k_{z_2,p})} + \frac{f_2'(0)}{(k_{z_2}-k_{z_2,p})^2}\right) \quad (33)$$

which can be simplified via the identities

$$B_2(k_{z_2}) = \frac{1}{2} - \frac{1}{jd_2}\sum_{p=-\infty}^{\infty}\frac{1}{(k_{z_2}-k_{z_2,p})} = \frac{1}{2} + \frac{1}{2j}\cot\left[\frac{1}{2}d_2(\gamma_2 - k_{z_2})\right] \quad (34)$$

and

$$\frac{1}{d_2}\sum_{p=-\infty}^{\infty}\frac{1}{(k_{z_2}-k_{z_2,p})^2} = jB_2'(k_{z_2}). \quad (35)$$

Here, $B_2(k_{z_2})$ is defined in the first paragraph of Section IV-A and $B_2'(k_{z_2})$ is its derivative with respect to the argument. With (34) and (35), (33) becomes

$$I_2(k_{z_2}) \sim f_2(0)B_2(k_{z_2}) - jf_2'(0)B_2'(k_{z_2}). \quad (36)$$

The diffracted fields arising from the truncation at $z_2 = 0$ are obtained from the saddle point at $k_{z_2} = k_{z_2}^s = z_2 k_{\rho_1,q}/\rho_1$ where $\rho_1 = (z_2^2 + y^2)^{1/2}$ is the transverse distance from edge 1 as shown in Fig. 1. The SBC of the diffracted field from edge 1 is obtained by evaluating the slowly varying function $f_1(z_{1q}(k_{z_2}))$ at the saddle point $k_{z_2} = k_{z_2}^s$. This leads to $f_1(z_{1q}^{d,1})$, with $z_{1q}^{d,1} = z_{1q}(k_{z_2}^s) = z_1 - \rho_1 k_{z_1,q}/k_{\rho_1,q} = z_1 - \rho_1\cos\beta_{1,q}/\sin\beta_{1,q}$ denoting the footprint of the qth edge-diffracted field. For approximate evaluation of the corresponding z_2-edge diffracted fields in (31), uniform asymptotics is necessary since $B_2(k_{z_2})$ and $B_2'(k_{z_2})$ have pole singularities of order 1 and 2, respectively, at $k_{z_2} = k_{z_2,p}$, which may lie near the saddle point. The uniform asymptotics is obtained by mapping the integral onto the two simplest canonical functions that match the same type of pole singularity and saddle points. To this end, we use the mathematical identities [10]

$$\int_{-\infty}^{\infty}\frac{e^{-Ks^2}}{s-y}\,ds = -\sqrt{\frac{\pi}{K}}\frac{F(jKy^2)}{y} \quad (37)$$

$$\int_{-\infty}^{\infty}\frac{e^{-Ks^2}}{(s-y)^2}\,ds = \frac{d}{dy}\int_{-\infty}^{\infty}\frac{e^{-Ks^2}}{s-y}\,ds = -\sqrt{\frac{\pi}{K}}\frac{d}{dy}\frac{F(jKy^2)}{y} \quad (38)$$

where $F(x)$ is the conventional UTD transition function [13] defined in (15), thereby matching the contributions in (36) that contain single poles (associated with $B_2(k_{z_2})$) and double poles (associated with $B_2'(k_{z_2})$). By using the identity $(d/d\xi)(F(\xi^2))/(\xi) = -(F_s(\xi^2))/(\xi^2)$, derived through direct differentiation from (15) and (16), one can express (39) in terms of the UTD slope transition function $F_s(x)$ defined as [14]

$$\frac{x}{j\sqrt{K\pi}}\int_{-\infty}^{\infty}\frac{e^{-Ks^2}}{\left(s-\sqrt{\frac{x}{jK}}\right)^2}\,ds = F_s(x). \quad (39)$$

Using (36) and (39), a locally uniform asymptotic evaluation of (31) is performed via SDP integration through the saddle point at $k_{z_2} = k_{z_2}^s$, leading to (14) where the exponential function arises from the evaluation of the integrand of (31) at the saddle point, i.e., $\mathbf{k}_q(k_{z_2}^s) = \mathbf{k}_q^{d,1}$.

APPENDIX II
THE VERTEX-RELATED TRANSITION FUNCTIONS T_h

In this Appendix, we provide the derivation of (23) and (24), which are useful for the numerical evaluation of the integral functions T_h. For convenience, let us define $g_h = [(-1)^{m+l}a_q^{m+1}b_p^{l+1}]/[j\pi(1-w^2)^{(m+l+1)/(2)}]$ where the relationships between h and l, m are defined after (19). Furthermore, define the simple-pole functions $C_\xi = 1/[\xi - (a_q)/(\sqrt{1-w^2})], C_\eta = 1/[\eta - (b_p)/(\sqrt{1-w^2}])$ which yield corresponding double-pole functions by differentiation $\partial C_\xi/\partial\xi = C_\xi' = -1/[\xi-(a_q)/(\sqrt{1-w^2})]^2, \partial C_\eta/\partial\eta = C_\eta' = -1/[\eta-(b_p)/(\sqrt{1-w^2})]^2$. The functions T_1 and T_2 in (21) can then be rewritten as $T_1 = g_1\iint C_\xi C_\eta e^{jq}d\xi d\eta, T_2 = -g_2\iint C_\xi C_\eta' e^{jq}d\xi d\eta = -\int C_\xi I_\eta(\xi)e^{j\xi^2}d\xi$ (with $q = q(\xi,\eta) = (\xi^2 + 2w\xi\eta + \eta^2)$) where $I_\eta(\xi) = \int C_\eta'(\xi)e^{j(2w\xi\eta+\eta^2)}d\eta$. Integration by parts can reduce this last integral to $I_\eta(\xi) = -2j\int(w\xi+\eta)C_\eta e^{j(2w\xi\eta+\eta^2)}d\eta$ because $C_\eta e^{j(2w\xi\eta+\eta^2)}|_{-\infty}^{\infty}$ vanishes due to the denominator of C_η. This leads to

$$T_2 = 2jg_2\int_{-\infty}^{\infty}\int_{-\infty}^{\infty}(w\xi+\eta)C_\xi C_\eta e^{jq}\,d\xi d\eta. \quad (40)$$

Similarly, interchanging $a_q \leftrightarrow b_p$ (which implies $g_2 \leftrightarrow g_3$ and $\xi \leftrightarrow \eta$ in (40)), we obtain $T_3 = 2jg_3\int_{-\infty}^{\infty}\int_{-\infty}^{\infty}(w\eta+\xi)C_\xi C_\eta e^{jq}d\xi d\eta$.

We reduce the expressions for T_2 in (40) to a form that involves only T_1 and the UTD transition function $F(x)$. First, we use the identity $w\xi + \eta = (\eta - (b_p)/(\sqrt{1-w^2})) + (b_p)/(\sqrt{1-w^2}) + w(\xi - (a_q)/(\sqrt{1-w^2})) + (wa_q)/(\sqrt{1-w^2})$ that leads to the decomposition of T_2 as follows:

$$T_2 = 2jg_2\int_{-\infty}^{\infty}\int_{-\infty}^{\infty}\left[C_\xi + \frac{(b_p+wa_q)}{\sqrt{1-w^2}}C_\eta C_\xi + wC_\eta\right]e^{jq}\,d\xi d\eta. \quad (41)$$

Since $q = q(\xi,\eta) = (\xi^2 + 2w\xi\eta + \eta^2) = \xi^2(1-w^2) + (\eta + w\xi)^2 = \eta^2(1-w^2) + (\xi + w\eta)^2$, the η-integral in the first term

and the ξ-integral in the third term of (41) can be evaluated in closed form, while the second term reconstructs T_1 so that

$$T_2 = 2jg_2 \left[\sqrt{j\pi} \int_{-\infty}^{\infty} C_\xi e^{j\xi^2(1-w^2)} d\xi + \frac{(b_p + wa_q)}{\sqrt{1-w^2}} \frac{T_1}{g_1} + \sqrt{j\pi} \int_{-\infty}^{\infty} C_\eta e^{j(\eta^2(1-w^2))} d\eta \right] = 2j \left[\frac{-\pi j F\left(a_q^2\right)}{a_q} + \frac{(b_p + wa_q)}{\sqrt{1-w^2}} \frac{T_1}{g_1} - \frac{w\pi j F\left(b_p^2\right)}{b_p} \right] \quad (42)$$

The last equality in (42) involves use of (37) in the first and third terms on the right-hand side. After rearrangement, we obtain (23). The expression for T_3 is obtained from symmetry in (41). To obtain the canonical form of the transition function T_4 in (21), we first perform a_q-differentiation of T_2 (or b_p-differentiation of T_3), using (21)

$$\frac{\partial T_2}{\partial a_q} = \frac{T_2}{a_q} - \frac{g_4}{a_q} \int_{-\infty}^{\infty} \int_{-\infty}^{\infty} C'_\eta C'_\xi e^{jq} d\eta d\xi = \frac{T_2 - T_4}{a_q}. \quad (43)$$

Insertion of (42) into (43), and term by term differentiation thereafter, yields

$$T_4 = T_2 - \frac{2ja_qb_p}{1-w^2} \cdot \left[b_p \frac{\partial F\left(a_q^2\right)}{\partial a_q} - wT_1 - (b_p + wa_q) \frac{\partial T_1}{\partial a_q} + wF\left(b_p^2\right) \right]. \quad (44)$$

Use of the identities $(\partial F(a_q^2))/(\partial a_q) = (F(a_q^2) - F_s(a_q^2))/(a_q)$ and $(\partial T_1)/(\partial a_q) = (T_1 - T_3)/(a_q)$ in (44), followed by simple manipulations, leads to (24).

REFERENCES

[1] F. Capolino, M. Albani, S. Maci, and L. B. Felsen, "Frequency domain Green's function for a planar periodic semi-infinite phased array. Part I: Truncated Floquet wave formulation," *IEEE Trans. Antennas Propag.*, vol. 48, no. 1, pp. 67–74, Jan. 2000.

[2] ——, "Frequency domain Green's function for a planar periodic semi-infinite phased array. Part II: Diffracted wave phenomenology," *IEEE Trans. Antennas Propag.*, vol. 48, no. 1, pp. 75–85, Jan. 2000.

[3] F. Capolino, S. Maci, and L. B. Felsen, "Asymptotic high-frequency Green's function for a planar phased sectoral array of dipoles," *Radio Sci. Special Issue on 1998 URSI Int. Symp. Electromagnetic Theory"*, ser. , vol. 35, no. 2, pp. 579–593, Mar.–Apr. 2000.

[4] S. Maci, F. Capolino, and L. B. Felsen, "Green's function for a planar phased sectoral array of dipoles," *Wave Motion "Special Issue on Electrodynamics in Complex Environments"*, vol. 34, no. 3, pp. 263–279, Sep. 2001.

[5] F. Capolino, F. Mariottini, S. Maci, and L. Felsen, "Floquet wave diffraction theory for tapared planar strip array Green's function," *Elektrik "Special Issue on Complex EM Problems and Numerical Simulation Technique"*, vol. 10, no. 2, pp. 273–289, 2002.

[6] P. Nepa, P. H. Pathak, O. A. Civi, and H.-T. Chou, "A DFT based UTD ray analysis of the EM radiation from electtrically large antenna arrays with tapered distribution," in *Proc. IEEE AP-S/URSI Symp.*, Orlando, FL, Jul. 11–16, 1999, p. 85.

[7] F. Capolino, S. Maci, M. Sabbadini, and L. Felsen, "Large phased array on complex platform," presented at the Int. Conf. Electromagnetics Advanced Applications (ICEAA), Torino, Italy, Sep., 10–14 2001.

[8] A. Cucini, M. Albani, and S. Maci, "Truncated Floquet wave full-wave (T(FW)2) analysis of large periodic arrays of rectangular waveguides," *IEEE Trans. Antennas Propag.*, vol. 51, no. 6, pp. 1373–1385, Jun. 2003.

[9] ——, "Truncated Floquet wave full-wave (T(FW)2) analysis of large phased arrays of open ended waveguides with a non uniform amplitude excitation," *IEEE Trans. Antennas Propag.*, vol. 51, no. 6, pp. 1386–1394, Jun. 2003.

[10] L. B. Felsen and N. Marcuvitz, *Radiation and Scattering of Waves*. Englewood Cliffs, NJ: Prentice-Hall, 1973.

[11] A. Papoulis, *The Fourier Integral and Its Applications*. New York: McGraw-Hill, 1962.

[12] J. D. Kraus, *Electromagnetics*. New York: McGraw-Hill, 1984.

[13] R. G. Kouyoumjian and P. H. Pathak, "A uniform geometrical theory of diffraction for an edge in a perfectly conducting surface," *Proc. IEEE*, vol. 62, pp. 1448–1461, 1974.

[14] R. G. Kouyoumjian, "The geometrical theory of diffraction and its applications," in *Numerical and Asymptotic Techniques in Electromagnetics*, R. Mittra, Ed. New York: Springer-Verlag, 1975.

[15] P. C. Clemmow, *The Plane Wave Spectrum Representation of Electromagnetic Fields*. New York: Pergamon, 1966.

[16] F. Capolino and S. Maci, "Simplified, closed-form expressions for computing the generalized Fresnel integral and their application to vertex diffraction," *Microwave Opt. Tech. Lett.*, vol. 9, pp. 32–37, 1995.

[17] K. H. Hill, "A UTD solution to the EM scattering by the vertex of a perfectly conducting plane angular sector," Ph.D. dissertation, Dept. of Electrical Engineering, Ohio State Univ., 1990.

[18] F. Capolino and S. Maci, "Uniform high-frequency description of singly, doubly, and vertex diffracted rays for a plane angular sector," *J. Electromagn. Wave Applicat.*, vol. 10, pp. 1175–1197, 1996.

[19] F. Capolino, M. Albani, S. Maci, and R. Tiberio, "Double diffraction at a couple of coplanar skew wedges," *IEEE Trans. Antennas Propag.*, vol. 45, no. 8, pp. 1219–1226, Aug. 1997.

[20] M. Albani, F. Capolino, S. Maci, and R. Tiberio, "Diffraction at a thick screen including corrugations on the top face," *IEEE Trans. Antennas Propag.*, vol. 45, no. 2, pp. 277–283, Feb. 1997.

[21] D. S. Jones, "A uniform asymptotic expansion for a certain double integral," in *Proc. Royal Soc. Edin. (A)*, vol. 69, 1971, pp. 205–226.

[22] A. Polemi, A. Toccafondi, and S. Maci, "High-frequency Green's function for a semi-infinite array of electric dipoles on a grounded slab. Part I: Formulation," *IEEE Trans. Antennas Propag.*, vol. 49, no. 12, pp. 1667–1677, Dec. 2001.

[23] S. Maci, A. Toccafondi, A. Polemi, and L. B. Felsen, "High-frequency Green's function for a semi-infinite array of electric dipoles on an infinite grounded stratified slab. Part II: Spatial domain parameterization," *IEEE Trans. Antennas Propag.*, 2005, to be published.

[24] L. B. Felsen, S. Maci, A. Toccafondi, and A. Polemi, High-frequency Green's function for a semi-infinite array of electric dipoles on an infinite grounded stratified slab. Part III: Phased matched wave interaction and numerical results, in *IEEE Trans. Antennas Propag.*, 2005.

[25] F. Capolino and L. B. Felsen, "Frequency and time domain Green's functions for a phased semi-infinite periodic line array of dipoles," *IEEE Trans. Antennas Propag.*, vol. 50, no. 1, pp. 31–41, Jan. 2002.

[26] ——, "Short-pulse radiation by a sequentially excited semi-infinite periodic planar array of dipoles," *Radio Sci.*, vol. 38, Mar.–Apr. 2003.

[27] C. A. Balanis, *Antenna Theory Analysis and Design*. New York: Wiley, 1982.

[28] A. Neto, S. Maci, G. Vecchi, and M. Sabbadini, "A truncated Floquet wave diffraction method for the full-wave analysis of large phased arrays. Part I: Basic principles and 2-D case," *IEEE Trans. Antennas Propag.*, vol. 48, no. 4, pp. 594–601, Apr. 2000.

[29] ——, "A truncated Floquet wave diffraction method for the full-wave analysis of large phased arrays. Part II: Generalization to the 3-D case," *IEEE Trans. Antennas Propag.*, vol. 48, no. 4, pp. 601–611, Apr. 2000.

[30] O. A. Civi, P. H. Pathak, H. T. Chou, and P. Nepa, "A hybrid uniform geometrical theory of diffraction-moment method for efficient analysis of electromagnetic radiation/scattering from large finite planar arrays," *Radio Sci.*, vol. 35, no. 2, pp. 607–620, Mar.–Apr. 2000.

F. Mariottini (S'00–M'03) was born in Siena, Italy, in 1973. He received the Laurea degree in telecommunication engineering and the Ph.D. degree in electromagnetics from the University of Siena, in 2000 and 2003, respectively.

He is presently a Postdoctoral Researcher at the University of Siena. His research interests are concerned with electromagnetic theory and applications, in particular with high-frequency methods and analysis and design of printed array antennas.

F. Capolino (S'94–M'97–SM'04) was born in Florence, Italy, in 1967. He received the Laurea degree *(cum laude)* in electronic engineering and the Ph.D. degree from the University of Florence in 1993 and 1997, respectively.

From 1994 to 2000, he was a Lecturer of antennas at the Diploma di Laurea, University of Siena, Italy, where he was a Research Associate until 2002 and is presently an Assistant Professor. From 1997 to 1998, he was a Fulbright Research Visitor with the Department of Aerospace and Mechanical Engineering, Boston University, Boston, MA, where he continued his research with a Grant from the Italian National Council for Research (CNR) from 1998 to 1999. From 2000 to 2001, he was a Research Associate and Visiting Professor with the Department of Electrical and Computer Engineering, University of Houston, Houston, TX, where he is now an Adjunct Assistant Professor. In November and December 2003, he was an Invited Assistant Professor at the Institut Fresnel, Marseille, France, working on EBG antennas. He is the coordinator of the Siena Unit for the Network of Excellence "Metamorphose" on Metamaterials of the sixth framework program of the European Union. His research interests include theoretical and applied electromagnetics focused on high-frequency short-pulse radiation, array antennas, periodic structures, numerical modeling, and metamaterials.

Dr. Capolino received an MMET'94 Student Paper Award in 1994, the Raj Mittra Travel Grant for Young Scientists in 1996, the "Barzilai" prize for the best paper at the National Italian Congress of Electromagnetism (XI RiNEm) in 1996, and a Young Scientist Award at the URSI International Symposium on Electromagnetic Theory in 1998. He received the R. W. P. King Prize Paper Award from the IEEE Antennas and Propagation Society for the best paper of 2000 by an author under the age of 36. He is an Associate Editor for the IEEE TRANSACTIONS ON ANTENNAS AND PROPAGATION.

S. Maci (M'92–SM'99–F'04) was born in Rome, Italy. He received the Laurea degree *(cum laude)* in electronic engineering from the University of Florence, Italy, in 1987.

From 1990 to 1998, he was with the Department of Electronic Engineering, University of Florence, as an Assistant Professor. Since 1996, he has been responsible for the University of Siena, Siena, Italy, projects supported by the European Community and the European Space Agency. In 1997, he was an Invited Professor at the Technical University of Denmark, Copenhagen. In 1998, he joined the Department of Information Engineering, University of Siena, as an Associate Professor. He is currently responsible for several research contracts and projects supported by national and international institutions. In the sixth EU framework program he is responsible of the European School of Antennas of the Antenna Center of Excellence. He is the principal author or co-author of about 40 papers in IEEE TRANSACTIONS, 40 papers in other international journals, and more than 200 papers in proceedings of international conferences. He was co-author of an incremental theory of diffraction, which describes a wide class of electromagnetic scattering phenomena at high frequency, and of a diffraction theory for the high-frequency analysis of large truncated periodic structures. His research interests are focused on electromagnetic engineering, mainly concerned with high-frequency ad numerical methods for antennas and scattering problems.

Prof. Maci is a Member of the Technical Advisory Board of the International Scientific Radio Union (URSI) Commission B, and the Advisory Board of the Italian Ph.D. School of Electromagnetism. He received the "Barzilai" prize for the best paper at the Italian National Electromagnetic Conference (XI RiNEm) in 1996. He was Associate Editor of the URSI disk of reference from 1996 to 1999, Associate Editor of IEEE TRANSACTIONS ON ELECTROMAGNETIC COMPATIBILITY from 1999 to 2001, and Convenor at the URSI General Assembly in 2002. He was Chairman and Organizer of several special sessions at international conferences and has been Chairman of two international workshops. He was a Guest Editor of the IEEE TRANSACTIONS ON ANTENNAS AND PROPAGATION *Special Issue on Artificial Magnetic Conductors, Soft Hard Surfaces, and Other Complex Surfaces*.

L. B. Felsen (S'47–M'54–SM'55–F'62– LF'90) was born in Munich, Germany, on May 7, 1924. He received the B.E.E., M.E.E, and D.E.E. degrees from the Polytechnic Institute of Brooklyn, Brooklyn, NY, in 1948, 1950, and 1952, respectively.

He emigrated to the United States in 1939 and served in the U.S. Army from 1943 to 1946. After 1952, he remained with the Polytechnic (now Polytechnic University), gaining the position of University Professor in 1978. From 1974 to 1978, he was Dean of Engineering. In 1994, he resigned from the full-time Polytechnic faculty and was granted the status of University Professor Emeritus. He is now Professor of Aerospace and Mechanical Engineering and Professor of Electrical and Computer Engineering at Boston University, Boston, MA (part-time). He is the author or coauthor of over 350 papers and of several books, including the classic *Radiation and Scattering of Waves* (Piscataway, NJ: IEEE Press, 1994). He is an associate editor of several professional journals and was an editor of the Wave Phenomena Series (New York: Springer-Verlag). His research interests encompass wave propagation and diffraction in complex environments and in various disciplines, high-frequency asymptotic and short-pulse techniques, and phase-space methods with an emphasis on wave-oriented data processing and imaging.

Dr. Felsen is a Member of Sigma Xi and a Fellow of the Optical Society of America (OSA) and the Acoustical Society of America. He has held named Visiting Professorships and Fellowships at universities in the United States and abroad, including the Guggenheim in 1973 and the Humboldt Foundation Senior Scientist Award in 1981. In 1974, he was an IEEE/APS (Antennas and Propagation Society) Distinguished Lecturer. His Poet's Corner appears sporadically in the IEEE/APS Magazine. He received the IEEE/APS Best Paper Award in 1969, and was coauthor for 1974 and 1981; he was contributing author to papers selected for the R.W.P. King Award for 1984, 1986, and 2000. Moreover, he received the Balthasar van der Pol Gold Medal from the International Union of Radio Science (URSI) in 1975, an honorary doctorate from the Technical University of Denmark in 1979, the IEEE Heinrich Hertz Gold Medal for 1991, the APS Distinguished Achievement Award for 1998, the IEEE Third Millenium Medal in 2000 (nomination by APS), an honorary Laurea degree from the University of Sannio in Benevento, Italy, in 2003, the IEEE Electromagnetics Award for 2003, an honorary doctorate from the Technical University of Munich, Germany, in 2004, three Distinguished Faculty Alumnus Awards from Polytechnic University, and an IEEE Centennial Medal in 1984. In 1977, he was elected to the National Academy of Engineering. He has served on the APS Administrative Committee from 1963 to 1966, and was Vice Chairman and Chairman for both the United States (1966–1973) and the International (1978–1984) URSI Commission B.